Ocean Science Journal (2022) 57:345–356
https://doi.org/10.1007/s12601-021-00052-w

Online ISSN 2005-7172
Print ISSN 1738-5261

ARTICLE

Origin of the Holocene Sediments in the Ninetyeast Ridge of the Equatorial Indian Ocean

Inah Seo[1,2] · Boo-Keun Khim[3] · Hyen Goo Cho[4] · Youngsook Huh[5] · Jongmin Lee[6] · Kiseong Hyeong[7]

Received: 25 August 2021 / Revised: 23 November 2021 / Accepted: 26 November 2021 / Published online: 21 January 2022

Abstract

The long-term evolution of the South Asian monsoon system and its influence on the Bay of Bengal (BOB) is of great interest to climate scientists. A number of climate forcings trigger the changes of the Indian summer monsoon (ISM) precipitation centroid, while the ISM rainfall projected by climate models shows a large discrepancy in local precipitation patterns. Moreover, the continuous recovery of paleoceanographic records in the BOB is often a struggle due to the presence of the fan-dominated depositional regime of the Bengal Fan. In this study, we present multi-proxy records of the last 13 kyrs from a sediment core (HI1710-MC1) at the Ninetyeast Ridge (NER) in the southern BOB, which is prevented from turbidite deposition. Our result suggests that the surface ocean environment and detrital provenance at the NER have not responded sensitively to the ISM variation and largely remained stable for the last 13 kyrs. The biogenic fraction ($CaCO_3$, total organic carbon, and total nitrogen contents) has remained relatively constant regardless of the Indian monsoon variability during the Holocene. The radiogenic isotope (ε_{Nd} and $^{87}Sr/^{86}Sr$) and clay mineral compositions of the detrital sediments indicate that the two major sources (the Himalaya through the Ganges–Brahmaputra–Meghna River system with a minor contribution from the Indo-Burma Ranges via the Irrawaddy-Salween River system) have played a primary role in delivering sediments to the study site. Our results imply that the longer sediment records preserved at the NER can be used to reconstruct the relative changes of runoff in the two major river systems. The Holocene record at the NER, thus, provides a basis for the study of the Late Quaternary variability in the Indian monsoon precipitation patterns and resultant runoff to the BOB.

Keywords Bay of Bengal · Clay mineral · Ninetyeast Ridge · Provenance · Sr–Nd isotopes

✉ Kiseong Hyeong
kshyeong@kiost.ac.kr

1 Department of Earth and Environmental Sciences, Jeonbuk National University, Jeonju 54896, Republic of Korea

2 Department of Environment and Energy, Jeonbuk National University, Jeonju 54896, Republic of Korea

3 Department of Oceanography, Pusan National University, Busan 46241, Republic of Korea

4 Department of Geology and Research Institute of Natural Science, Gyeongsang National University, Jinju 52828, Republic of Korea

5 School of Earth and Environmental Sciences, Seoul National University, Seoul 08826, Republic of Korea

6 Deep-Sea Mineral Resources Research Center, Korea Institute of Ocean Science and Technology, Busan 49111, Republic of Korea

7 Global Ocean Research Center, Korea Institute of Ocean Science and Technology, Busan 49111, Republic of Korea

1 Introduction

The South Asian monsoon, characterized by the seasonal reversal of surface winds and associated precipitation (IPCC 2014), affects the lives of more than a billion people. Yet, the projections using state-of-the-art climate models exhibit a high degree of uncertainty in determining local precipitation. Accurately projecting future monsoonal variability and the changes in regional precipitation is thus difficult to achieve (Turner and Annamalai 2012). For this reason, a number of studies have used geological records to examine the responses of the South Asian monsoon to climate change. In particular, long-term changes in monsoonal runoff are estimated from the detrital flux in the Bengal Fan sediments (Hovan 1995; Galy and France-Lanord 2001; Ali et al. 2021).

The Bay of Bengal (BOB), the northeastern part of the Indian Ocean, receives a large amount of detritus from major

rivers draining the Himalayas (e.g., Ganges, Brahmaputra, and Meghna). However, the source of the sediments is not exclusive to the Himalayas as evidenced by differences in their radiogenic isotope (Sr–Nd) compositions (Colin et al. 1999; Joussain et al. 2016; Ali et al. 2021). Instead, a significant input of detritus from the Myanmar region (e.g., through the Irrawaddy and Salween rivers), where monsoon rainfall is particularly intense, is suggested based on the Sr–Nd compositions of the BOB sediments. The changes in the runoff of the major rivers in the BOB, therefore, can be estimated quantitatively by evaluating the detritus contribution to sedimentary records from various rivers with different drainage areas in the BOB. Nevertheless, the fan-dominated depositional processes of the central BOB often complicate the recovery of continuous, high-resolution sedimentary records. For this reason, the Ocean Drilling Program (ODP) and the International Ocean Discovery Program (IODP) drilled the Ninetyeast Ridge (NER) where the ridge-top location of the NER has prevented the turbiditic sediment input and the resultant truncation of the underlying sequence: ODP Site 758 and IODP Site U1443 (5° 23.05′ N, 90° 21.67′ E) (Pierce et al. 1989; Clemens et al. 2016; see locations in Fig. 1). According to the paleoceanographic variability and the detrital input from the Himalayan erosion for the late Neogene (Gourlan et al. 2010; Bolton et al. 2013; Ali et al. 2021; Bretschneider et al. 2021), these sites are governed by the Indian monsoon regime's precipitation and open-ocean dynamics regulated by its current system.

We collected two multiple cores (34 cm- and 35-cm long) at the northern NER using the R/V ISABU of the Korea Institute of Ocean Science and Technology (KIOST, launched in 2017) during the 2017 research cruise in the Indian Ocean (project title: Marine environmental change and the evolution of Indian monsoon). To investigate the surface ocean environment and the provenance of the detrital components, we used the multi-proxy dataset from the 35-cm long undisturbed multiple core. We evaluated the origin of the study site's biogenic sediment and compared the analyzed radiogenic isotope ($^{143}Nd/^{144}Nd$ and $^{87}Sr/^{86}Sr$) and clay mineral compositions of detrital components to those of the adjacent basins (i.e., the BOB and Andaman Sea). We addressed the provenance and the relative contribution of the Himalayan and Myanmar detrital components during the Holocene. This study provides background data for the reconstruction of changes of runoff in the major river systems under the influence of the Indian monsoon system.

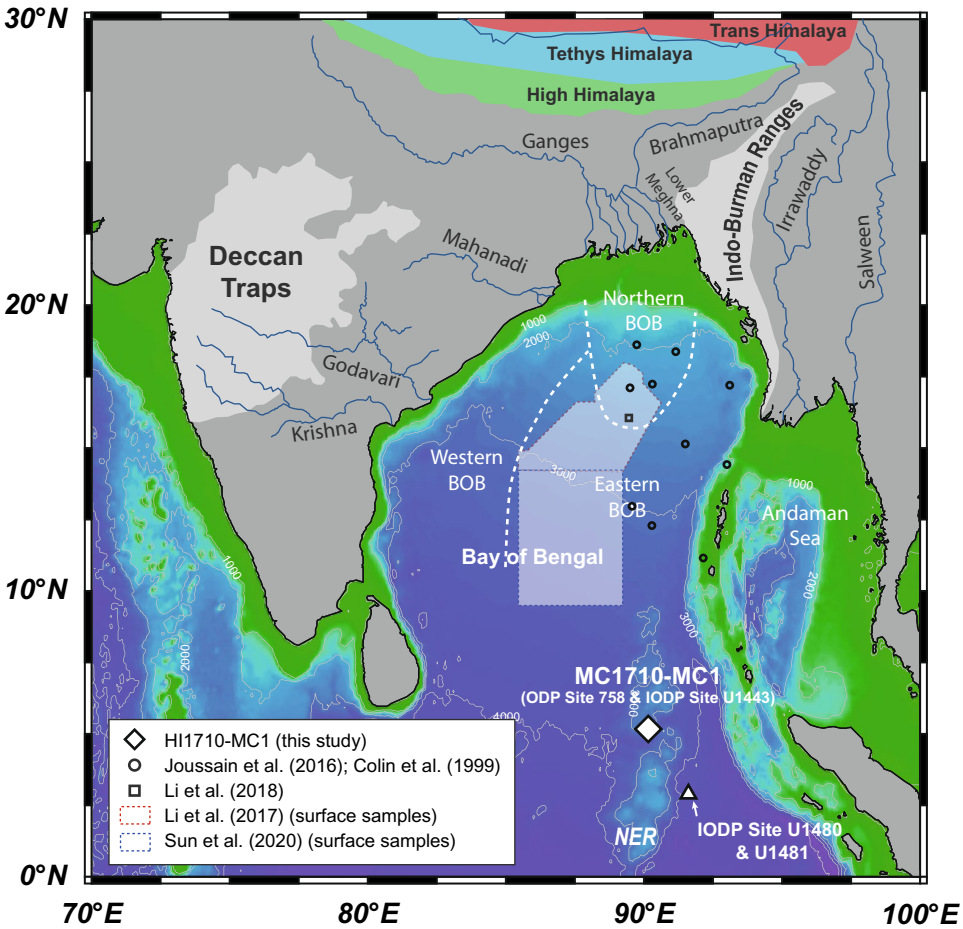

Fig. 1 Core location of HI1710-MC1 and schematic map of surrounding area. The study sites of cited literature are also shown (see legend) with provinces suggested by Colin et al. (1999). The map was generated with Ocean Data View software (Schlitzer 2020) using 6′×6′ gridded bathymetry data from GEBCO 2014 database (https://www.gebco.net/data_and_products/gridded_bathymetry_data/) and modified based on Ali et al. (2021). *NER* Ninetyeast Ridge, *BOB* Bay of Bengal

The sedimentary records spanning the last 13 kyrs will serve as a baseline dataset for the long-term paleoceanographic reconstruction.

2 Study Site

A multiple core HI1710-MC1 (5° 23.010′ N, 90° 21.738′ E, 2925 m water depth) was collected from the NER in the BOB during the HI1710 expedition of the R/V ISABU in 2017 (Fig. 1). The NER formed before the middle Eocene by age-progressive hotspot volcanism that is currently beneath the Kerguelen Plateau (Royer et al. 1991; Sager et al. 2010; Clemens et al. 2016). The ridge-top location of the site allows preservation of a continuous sedimentary record suitable for paleoceanographic study. Further, the surface salinity at the study site remains relatively constant throughout the year despite the strong monsoonal precipitation, yielding exceptionally strong north–south salinity gradient and the seasonal variation in the local salinity of the BOB and Andaman Sea (Fig. 2). Thus, we considered this site to be at the southern limit influenced by the Indian summer monsoon.

3 Methods

The 35 cm-long multiple core was halved, photographed, and sectioned at 1-cm intervals at the Library of Marine Samples (LIMS), South Sea Branch, KIOST. The sectioned subsamples were stored in 50 mL plastic jars and then freeze-dried. To separate sand-sized foraminifera from the clay, approximately 1 g of bulk sediments was soaked in 5% sodium hexametaphosphate solution and then sieved using tap water into > 125 μm, 125–63 μm and < 63 μm fractions. More than 100 specimens of planktic foraminifera (mixed species) were isolated from the > 125 μm fraction of four selected intervals for an accelerator mass spectrometer (AMS) radiocarbon dating (Table 1). Radiocarbon age determinations were processed using an AMS at the Beta Analytics, USA and the Rafter Radiocarbon Laboratory of National Isotope Centre, New Zealand. Calibration of the radiocarbon ages was performed with the Calib 7.0 (http://calib.org) software and the Marine20 calibration curve (Stuiver and Reimer 1993; Heaton et al. 2020; Stuiver et al. 2021). The local reservoir effect (ΔR) of 17 ± 70 year was applied which was reported for Nicobar Island (9° N, 94° E) (Southon et al. 2002).

The surface ocean productivity was inferred from the biogenic components. The bulk sediment was dried at 50 °C and ground using mortar and pestle for the analyses of total carbon (TC), total inorganic carbon (TIC), and total nitrogen (TN) contents. The TC and TN contents of every subsample were measured with a Flash 2000 Series Elemental Analyzer at Pusan National University (PNU) and was reported as a percentage of sediment dry mass. The analytical precisions were less than ± 0.1% and ± 0.01%, respectively. The TIC content was measured with a UIC CM5012 CO_2 coulometer at PNU (Engleman et al. 1985). The analytical precisions were less than ± 0.1%. The TIC was multiplied by 8.333 (the molecular weight ratio between $CaCO_3$ and C) to calculate the calcium carbonate content. The TIC was subtracted from the TC to estimate the total organic carbon (TOC) content.

To investigate detrital provenance, the inorganic silicate fraction (hereafter the detrital fraction) was extracted from the bulk sediments using a method outlined by Hovan (1995) at KIOST. The < 63 μm sample was treated with a 10% acetic acid to remove the carbonate fraction. Subsequently, to remove Fe–Mn oxides and hydroxides, the sample was treated with a hot sodium citrate–sodium dithionite solution buffered with sodium bicarbonate. The biogenic silica component was then removed with an 80 °C sodium hydroxide solution. An analysis of the $^{143}Nd/^{144}Nd$ and $^{87}Sr/^{86}Sr$ ratios of bulk inorganic silicate fraction, including isotopic separation and multi-collector thermal ionization mass spectrometric (TIMS; VG54-30, Isoprobe-T) analysis, was performed at the Korea Basic Science Institute. The detailed methodology was outlined by Cheong et al. (2016). The replicate analysis of NBS987 and JNdi-1 provided the mean values of $^{143}Nd/^{144}Nd = 0.512110 \pm 20$ ($n = 5$, 2σ), $^{87}Sr/^{86}Sr = 0.710251 \pm 70$ ($n = 5$, 2σ). For convenience, we expressed the $^{143}Nd/^{144}Nd$ ratios as ε_{Nd}; i.e., the deviation from a chondritic uniform reservoir ($\varepsilon_{Nd} = (^{143}Nd/^{144}Nd/0.512638 - 1) \times 10^4$) (Jacobsen and Wasserburg 1980).

The clay mineralogy was determined from the < 2 μm clay fraction, which was separated according to the Stoke's Law, spread onto glass slides, and allowed to air dry. Analyses were performed on air-dried and ethylene glycol-treated mounts using the SIMENS/Bruker D5005 X-ray diffractometer with CuKα radiation in 40 kV, 40 mA, and 3–30° (2θ) conditions at the Department of Geology, Gyeongsang National University. The relative abundances of four major clay minerals (smectite, illite, kaolinite and chlorite) were semi-quantitatively estimated using the Eva 3.0 software with the empirical factors of Biscaye (1965). The relative proportions of kaolinite and chlorite were determined based on the ratio from the 3.58 Å (kaolinite 002) and 3.54 Å (chlorite 004) peak areas.

4 Results

The HI1710-MC1 sediments consisted of a homogeneous pale brown nannofossil ooze with foraminifera and clay without any noticeable lithological changes. Table 1 summarizes the analytical results of HI1710-MC1 sediment as shown in Fig. 3. Table 2 presents the four AMS

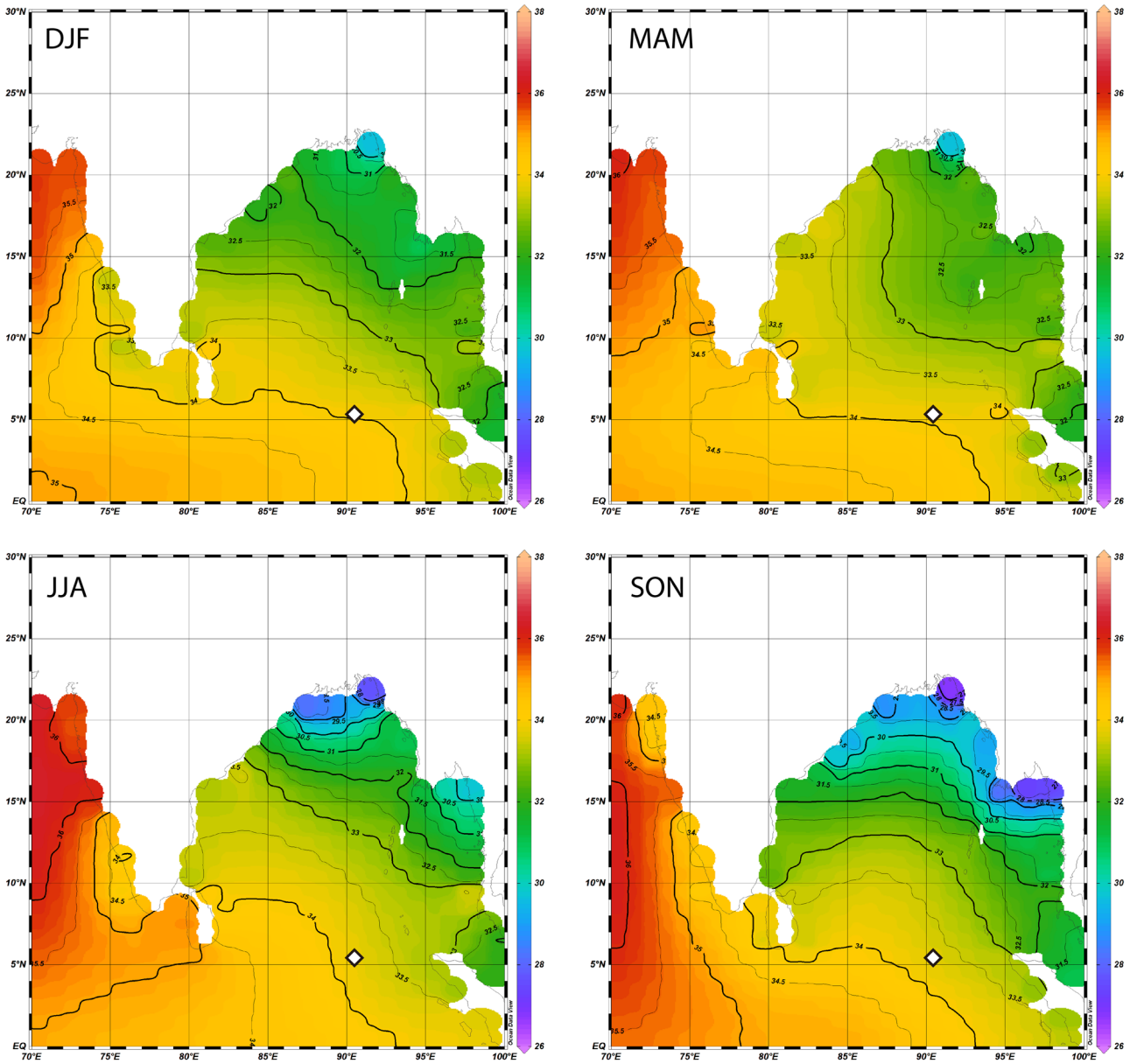

Fig. 2 Statistical mean salinity data on 1° grid for 1981–2010 from World Ocean Atlas 2018 (Zweng et al. 2018). The study site (HI1710-MC1) is shown as an open diamond (*DJF* December–January–February, *MAM* March–April–May, *JJA* June–July–August, *SON* September–October–November)

^{14}C dates of planktic foraminifera. The core extended to 14,213 cal yr before present (BP), and the average linear sedimentation rate (LSR) of the composite section was estimated to be 2.4 cm/kyr. The increase in LSR in the uppermost layer (Fig. 3a) is attributable to the high water content and minimal compaction. The age model was established using linear interpolation between measured intervals (Fig. 3a). The $CaCO_3$ contents ranged between 56.1 and 64.7 wt% (avg. 61.0 wt%) (Fig. 3b). The TOC and TN were remarkably low (< 0.5% and < 0.07%, respectively) and TN contents were below the limit of detection in several samples (Fig. 3c). The measured ε_{Nd} and $^{87}Sr/^{86}Sr$ varied between − 11.8 and − 12.4, and 0.7260 and 0.7289, respectively (Fig. 3d, e). The most common clay mineral in the < 2 μm fraction was illite (av. 50.1%), followed by smectite (av. 22.7%), kaolinite (av. 14.6%), and chlorite (av. 13.6%) (Fig. 3f). The relative abundance of each clay mineral group did not change significantly through the analyzed section.

Table 1 Analytical results of HI1710-MC1

Depth (cm)	Bulk contents					Bulk detrital isotope composition			Clay Mineralogy (%)			
	TC[a] (%)	TN[b] (%)	$CaCO_3$ (%)	TOC[c] (%)	TOC/TN	$^{87}Sr/^{86}Sr$	$^{143}Nd/^{144}Nd$	ε_{Nd}	Sm[d]	Il[e]	K[f]	Chl[g]
0–1	7.69	0.06	60.6	0.42	7.01				20.7	50.5	15.1	13.7
1–2	7.91	0.06	62.2	0.45	7.44	0.7260	0.512007	− 12.3				
2–3	8.08	0.06	63.7	0.44	7.54							
3–4	7.94	0.06	62.3	0.46	8.29							
4–5	8.19	0.05	64.6	0.43	8.40				24.5	45.6	16.3	13.5
5–6	8.01	0.05	63.0	0.45	8.50							
6–7	7.86	0.06	61.9	0.43	7.73							
7–8	7.88	0.05	63.1	0.31	6.39							
8–9	7.83	0.05	63.1	0.26	5.37							
9–10	7.84	0.04	64.7	0.07	1.58	0.7266	0.512030	− 11.9	18.4	53.7	14.4	13.4
10–11	7.58	0.04	61.6	0.19	4.55							
11–12	7.55	0.04	61.1	0.22	5.39							
12–13	7.54	0.04	60.8	0.25	5.75							
13–14	7.38	0.04	60.8	0.08	2.14							
14–15	7.48	BDL[h]	61.2	0.14	–				25.4	47.0	15.9	11.8
15–16	7.59	BDL	61.2	0.24	–							
16–17	7.61	0.04	61.3	0.25	6.84							
17–18	7.33	0.04	59.7	0.16	3.98							
18–19	7.35	0.04	59.4	0.22	6.04							
19–20	7.40	0.04	61.4	0.03	0.78	0.7284	0.512000	− 12.4	26.2	44.6	15.2	14.1
20–21	7.15	0.04	57.9	0.19	5.45							
21–22	6.99	0.04	56.1	0.25	7.02							
22–23	7.75	BDL	64.6	–	–							
23–24	7.34	0.04	59.7	0.17	3.97							
24–25	7.12	0.04	58.3	0.13	3.81	0.7289	0.512024	− 12.0	23.1	50.6	13.9	12.4
25–26	7.06	0.03	58.4	0.05	1.38							
26–27	7.08	0.03	57.8	0.15	4.22							
27–28	7.12	BDL	59.0	0.04	–							
28–29	7.29	0.03	59.7	0.13	3.97							
29–30	6.97	0.03	57.4	0.08	2.27	0.7286	0.512028	− 11.9	18.8	54.3	12.7	14.3
30–31	7.47	0.04	61.9	0.04	1.19							
31–32	7.38	BDL	62.1	–	–							
32–33	7.50	BDL	61.7	0.09	–							
33–34	7.52	BDL	62.5	0.02	–	0.7286	0.512034	− 11.8				
34–35	7.35	0.03	60.5	0.09	2.82				16.8	54.1	13.6	15.5

[a]Total carbon; [b]total nitrogen; [c]total organic carbon; [d]smectite; [e]illite; [f]kaolinite; [g]chlorite; [h]BDL: below detection limit

5 Discussion

5.1 Surface Ocean Environment at the Ninetyeast Ridge

The $CaCO_3$ content in marine sediment shows spatial and temporal variation which reflects its production, preservation, and dilution by non-carbonate materials (Arrhenius 1952; Farrell and Prell 1989; Naidu et al. 1993). In the BOB, the sediment discharged from the major rivers (e.g., the Ganges–Brahmaputra, Irrawaddy, etc.) often exert a major control on the $CaCO_3$ concentration in marine sediment, especially at the sites proximal to the continent or under the influence of the submarine fan deposition (Kolla et al. 1976; Suresh and Bagati 1998). For instance, the $CaCO_3$ content at the western BOB sites close to the Indian continent is low (generally < 10%) during the Holocene, but it was higher during the last glacial maximum (LGM). This is due to the weakened summer monsoon and the resultant decrease in sediment discharge (Suresh and Bagati 1998; Phillips et al. 2013). Such effect of terrigenous dilution decreases greatly toward the offshore area as inferred

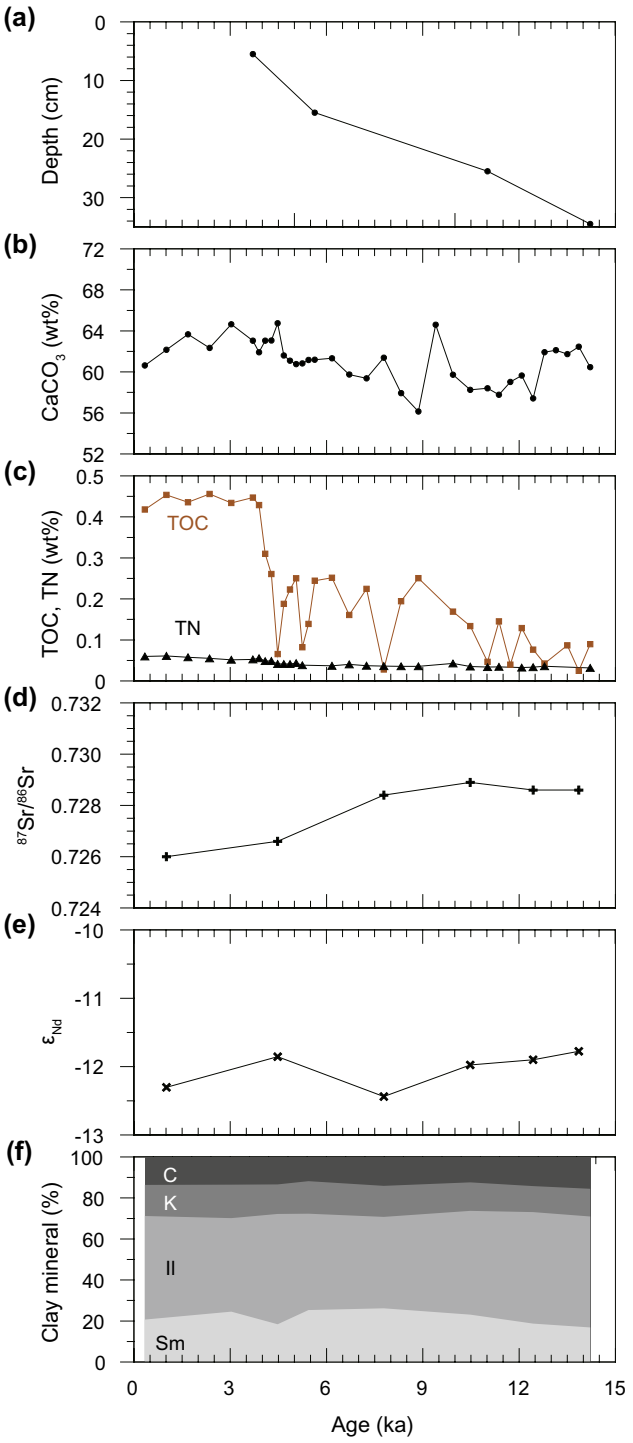

Fig. 3 Analytical results of HI1710-MC1 plotted against depth. **a** Depositional ages, **b** $CaCO_3$ content, **c** total organic carbon (TOC) and total nitrogen (TN) contents, **d** $^{87}Sr/^{86}Sr$ of lithogenic component, **e** ε_{Nd} of lithogenic component and **f** clay mineral assemblages. *C* chlorite, *K* kaolinite, *Il* illite, *Sm* smectite

from the reduced contribution of the lithogenic component in suspended sediments (e.g., Rixen et al. 2019), and it is often considered insignificant in the central ocean basin.

Table 2 AMS radiocarbon ages of selected intervals for HI1710-MC1

Depth (cm)	Conventional ^{14}C Age (year)[a]	Cal yr B.P.[b]	Laboratory
5–6	3921 ± 26	3582–3823	Rafter Radiocarbon
15–16	5466 ± 28	5523–5740	Rafter Radiocarbon
25–26	10,111 ± 36	10,877–11,153	Rafter Radiocarbon
34–35	12,730 ± 50	14,036–14,391	Beta Analytics

[a,b] One sigma ranges

Carbonate dissolution has been considered as a significant control on the $CaCO_3$ content as well, especially in the carbonate-undersaturated deep ocean (e.g., Peterson and Prell 1985).

The $CaCO_3$ content of HI1710-MC1, obtained from the central ocean ridge, does not vary greatly for the last 14.4 kyrs (Fig. 3b). Minor variability in centimeter scale could be attributed to the millennial- or centennial-scale climate variability (e.g., 8.2 ka event; Banerji et al. 2020); however, the low sedimentation rate (ca. 2.4 cm kyr^{-1}) at the study site does not resolve such events precisely. Still, $CaCO_3$ was lower in the 17–30 cm interval, which corresponded to the depositional ages of 6–11 ka. As previously determined carbonate preservation state at the NER sites suggested that the dissolution maxima have often occurred at the glacial initiations (Peterson and Prell 1985), this early- to mid-Holocene minimum is not attributable to the carbonate dissolution. Instead, this time period is marked by a strengthened ISM precipitation (Fleitmann et al. 2003; Hong et al. 2003). Thus, the observed $CaCO_3$ decrease probably indicates an increased terrigenous dilution during the early- to mid-Holocene. Overall, the $CaCO_3$ content was rather high (avg. 61.0%) compared to those (0–50%) from the surrounding basin of the BOB (Kolla et al. 1976). This indicates that the ISM-related river discharge is not particularly distinctive in the bulk composition of HI1710-MC1 throughout the study period. The other biogenic components, the TOC and TN contents, were very low (< 0.5%) and decreased downcore (Fig. 3c). This tendency is not attributed to the paleoproductivity change, but to the decay of organic material (i.e., remineralization) after burial. The strong correlation of the TOC with the TN ($r = 0.88$, $p < 0.001$) suggests their common origin. The TOC/TN (C/N) ratios were lower than ten throughout the core, indicating the aquatic (marine) origin of the organic matter (Meyers 1994).

The small influence of terrigenous dilution on the $CaCO_3$ variation, the low C/N ratio of organic material, and the low linear sedimentation rate (*ca.* 2.4 cm/kyr) imply that there is only a minor control of river discharge from the regional surface ocean environment, which is also supported by the small seasonal variability of sea surface salinity between 33.5 and 34.0 psu (Fig. 2). Bolton et al. (2013) found the

diminished upper water column stratification at the NER site (ODP site 758) during the ISM strengthening events with an analysis of a 500,000-year foraminifera oxygen isotope record. Such phenomenon in the central BOB does not correspond to the enhanced surface water stratification in the northern BOB and Andaman Sea sites, indicated by the approximated decrease in sea surface salinity, during the strengthening of ISM in the mid-Holocene (Gebregiorgis et al. 2016; Sijinkumar et al. 2016). Our results support Bolton et al. (2013)'s suggestion that the large-scale surface wind system and ocean dynamics, rather than regional land–ocean interaction represented by freshwater discharge, largely regulates the surface ocean environment at the NER.

5.2 Detrital Provenance During the Holocene: 1. Sr–Nd Isotope

The Sr–Nd radiogenic isotope compositions of detrital sediments are useful indicators of sediment provenance (e.g., Nakai et al. 1993; Chen et al. 2007; Chen and Li 2013). Although the Himalayas produces an enormous amount of detritus, which is supplied to the entire BOB, the geology of catchment areas of individual river systems is different from one another. This results in the regional variation of BOB detrital sediment in their composition. For instance, the Ganges–Brahmaputra-lower Meghna (G-B-M) rivers mainly drain the Himalayas, whereas the Irrawaddy and Salween (I-S) rivers incorporate detritus from the Indo-Burma Ranges (IBR), Myanmar Central Basin, and Shan Plateau. According to the earlier work by Colin et al. (1999), the Eastern Indian Ocean was divided into four provinces based on the detrital Sr–Nd and clay mineralogy: the northern BOB, the western BOB, the eastern BOB, and the Andaman Sea (Figs. 1 and 4) (Colin et al. 1999; Gourlan et al. 2010; Tripathy et al. 2011; Ali et al. 2021). The western BOB sediments, including the samples from the levee of an active channel of the Bengal Fan (Tripathy et al. 2011; Lupker et al. 2013), are characterized by Nd–Sr isotope composition similar to that of the Lower Meghna river developed downstream of the Ganges and Brahmaputra river confluence (Fig. 4). This suggests the dominance of detritus supplied by these rivers in the western BOB. The western BOB is also fed by the peninsular rivers of India draining into the Archean Shield (e.g., Godavari and Krishna) represented by ε_{Nd} and $^{87}Sr/^{86}Sr$ signatures similar to G-B-M rivers (Fig. 4). However, sediment discharge of these rivers is much smaller (ca.

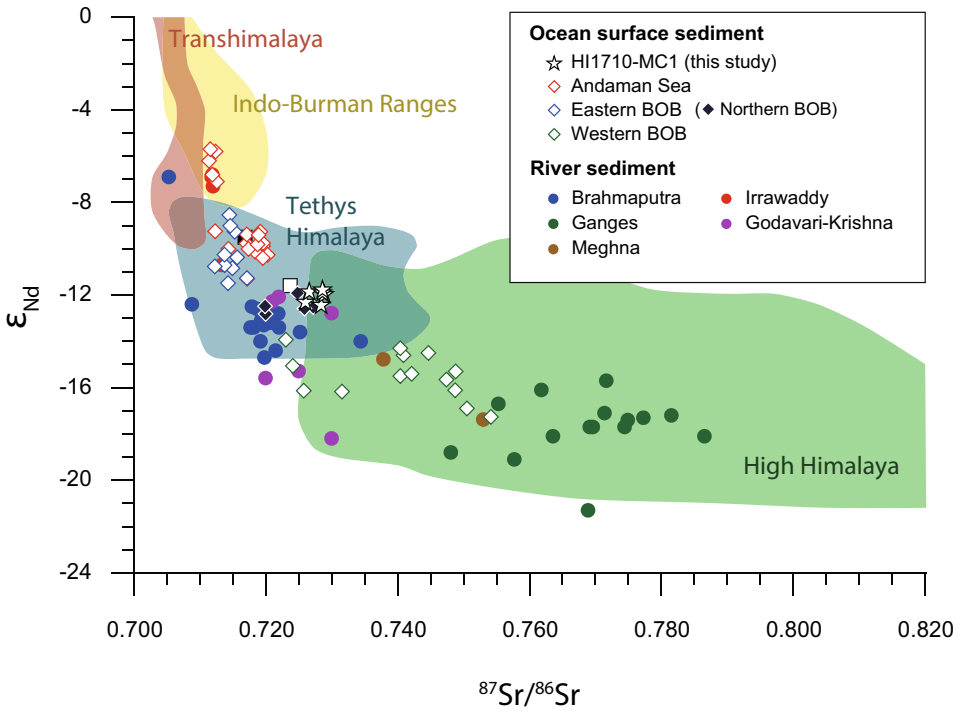

Fig. 4 Crossplot for $^{87}Sr/^{86}Sr$ and ε_{Nd} of lithogenic component of HI1710-MC1. Compositions of surface sediments, including Holocene sediment in Bay of Bengal and Andaman Sea are also shown (Colin et al. 1999; Ahmad et al. 2009; Tripathy et al. 2011; Lupker et al. 2013; Ali et al. 2015; Joussain et al. 2016; Miriyala et al. 2017) (Supplementary Table A1). Composition of the bulk detrital (Gourlan et al., 2010) and clay (<2 μm) fraction from the uppermost interval of the ODP Site 758 are shown as open and closed squares, respectively (Ali et al. 2021; Song et al. 2021). The average compositions of major river sediments and possible source regions (shaded area) are shown together and provided as supplementary data (Galy and France-Lanord 2001; Singh and France-Lanord 2002; Allen et al. 2008; Najman et al. 2008; Singh et al. 2008; Gourlan et al. 2010; Licht et al. 2013; Giosan et al. 2018; Ali et al. 2021)

10%) compared to G-B-M rivers (Mouyen et al. 2018). The influence of sediments from the mainland India is considered insignificant in the entire western BOB, as also supported by clay mineral composition discussed in the next section.

The eastern BOB and the Andaman Sea sediments are characterized by more radiogenic Nd and less radiogenic Sr isotope signatures than those of the western BOB sediments (Fig. 4). This was attributed to the input of IBR sediments with radiogenic Nd and unradiogenic Sr signatures that were discharged into the Andaman Sea shelf and the easternmost part of the BOB via the I-S rivers (Colin et al. 1999; Joussain et al. 2016; Ali et al. 2021; Bretschneider et al. 2021). While the I-S rivers are known to discharge mostly in the Andaman Sea (Colin et al. 1999; Ali et al. 2015; Lee et al. 2020), the appearance of intermediate Nd–Sr isotope compositions, between the Andaman Sea and the western BOB sediments, suggests significant input of sediments from the I-S rivers to the eastern BOB (Fig. 4). Even the northern BOB sediments, sampled near the G-B-M river mouth, reveal isotopic compositions between the eastern BOB and Meghna river sediments (Fig. 4). This suggests that the I-S and IBR components have influence in the wide region of the eastern BOB.

The Sr and Nd isotope compositions of HI1710-MC1 are similar to those of northern BOB sediment (Fig. 4), an indication of their common source area, which is primarily the High and Tethys Himalaya and secondarily the IBR regions. The heavy monsoonal precipitation on the eastern Himalaya and IBR regions allows intense sediment discharge through I-S rivers, which is comparable (~ 70%) to those of G-B-M river system (Chapman et al. 2015). Although most of them would be primarily deposited into the Andaman Sea basin, a significant amount of I-S river sediments is transported to the eastern BOB (Ali et al. 2021; Bretschneider et al. 2021). Ours and the northern BOB samples had less radiogenic ε_{Nd} and more radiogenic $^{87}Sr/^{86}Sr$ than those of the eastern BOB sediments, which indicate the smaller contribution of the I-S river sediments in the remote area from the Irrawaddy river mouth. Our Nd–Sr isotope data suggest that the G-B-M river system with secondary input from I-S river system strongly influences the northern and eastern BOB, including the NER.

Eolian mineral dust and volcanic materials might have been supplied to the study site as minor component. The modern dust deposition in the southern BOB is estimated as 0.1–0.2 g cm^{-2} ky^{-1} by dust models (Jickells et al. 2005), which seems significant compared to the total lithogenic flux of 0.2–0.8 g cm^{-2} ky^{-1} during the Late Quaternary measured in the deep-sea sediments at the adjacent ODP Site 758 (5° 23.05′ N, 90° 21.67′ E; Hovan and Rea 1992; Song et al. 2021). Dust supplied to the surface ocean is, however, subjected to the various internal processes (e.g., biological scavenging, chemical degradation, physical advection, etc.), so as not to be fully exported to the bottom. For instance, the measured inorganic silicate deposition flux at the northeastern Pacific site (KODOS 02-01-02, 16° 12′ N, 125° 59′ W), where the terrigenous mineral transport is nearly dominated by the eolian process, was 0.012 g cm^{-2} ky^{-1} (Hyeong et al. 2006). This is significantly below the model estimation of 0.02–0.05 g cm^{-2} ky^{-1} (Jickells et al. 2005). In this context, the actual amount of dust deposition at the study site is likely to be much lower than the model estimation. The amount of volcanic material from the adjacent Sunda arc would be very minor in the NER as well, as volcanic detritus is rarely found, even at the arc-proximal Nicobar Fan sites (IODP Site U1480 and U1481; see locations in Fig. 1) (Pickering et al. 2020). Given the tremendous amount of sediment input from the Himalaya, the BOB is primarily filled by riverine fluxes from the adjacent landmasses and the following hemipelagic processes, including deep-sea current, suspension-settling, etc.

5.3 Detrital Provenance During the Holocene: 2. Clay Mineralogy

Clay mineral assemblage can be used to estimate the relative contribution of sediment supplied by major rivers. The northern and eastern BOB surface sediments were plotted into two groups (EBOB-1 and EBOB-2) with distinct clay mineral compositions (Fig. 5). The clay mineral composition of the EBOB-2 group (Li et al. 2017, 2018; Sun et al. 2020) was estimated by applying the weighting factors of Biscaye (1965) for different minerals. All the samples in the EBOB-2 group plotted close to our data (Fig. 5), which is indicative of their common provenance. The clay mineral composition of another group (EBOB-1) that included the northern BOB sediments was estimated without the weighting factors of Biscaye (1965), and could not be compared with our data directly.

In the BOB, dominant clay minerals are illite and smectite with minor contribution of chlorite and kaolinite. The major sources of illite and smectite are the G-B-M and I-S river systems, respectively (Colin et al. 1999; Joussain et al. 2016; Khan et al. 2019; Sun et al. 2020). The G-B-M river system is the sole known source dominated by illite (Table 3). The dominance of illite over smectite in HI1710-MC1 sediment thus indicates a significant influence of the G-B-M rivers. If we assume G-B-M rivers and I-S rivers as the two major detrital sources, the clay mineral composition of HI1710-MC1 site can be explained with the mixing of ~ 70% of G-B-M river and ~ 30% I-S river sediments (Fig. 5), which agrees with the estimation based on Sr–Nd isotope compositions. However, the kaolinite/chlorite ratio (K/C) of 0.9 ~ 1.3 in our samples is not explained with mixing of two sources of G-B-M and I-S rivers with an average K/C ratio of 0.4 and 0.8, respectively, which indicates a minor influence of G-K

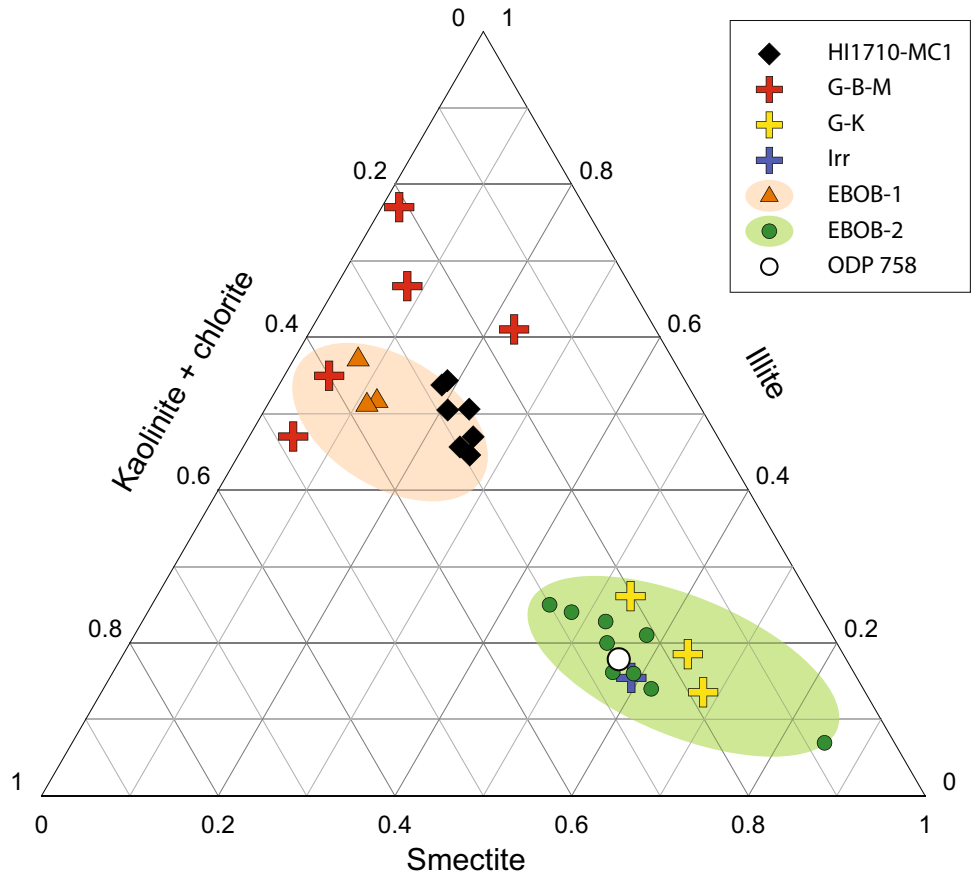

Fig. 5 Ternary diagram for clay mineral assemblages of HI1710-MC1 (solid diamonds) plotted together with the average compositions of river mouth and Bay of Bengal sediments. Irrawaddy: Irr, blue cross (Rodolfo 1969); Ganges–Brahmaputra-lower Meghna: G-B-M (Khan et al. 2019), red cross; Godavari-Krishna: G-K, yellow cross (Bejugam and Nayak 2017); eastern Bay of Bengal (BOB) surface sediment: green shade and green circles labelled as EBOB-1 (Colin et al. 1999; Joussain et al. 2016) and orange shade and triangles labelled as EBOB-2 and triangles (Li et al. 2017, 2018; Sun et al. 2020). Note the composition of ODP Site 758 sediment (open circle) (Ali et al. 2021) included in the EBOB-1 group (See Fig. 1 for sampling locations)

Table 3 Average clay mineral compositions of major rivers surrounding the Bay of Bengal (data adopted from Sun et al. (2020))

	Smectite	Illite	Kaolinite	Chlorite	Data source
Ganges–Brahmaputra–Meghna	8	66	8	17	Khan et al. (2019)
Godavari–Krishna	57.6	17.8	20.9	3.7	Bejugam and Nayak (2017)
Irrawaddy	59.0	15.5	11.6	13.9	Rodolfo (1969); Colin et al. (1999)

river sediments with an average K/C ratio of 5.6 (Table 3). Thus we cannot preclude influence of G-K river sediments that cannot be deciphered with Nd–Sr isotope composition because of similar composition between G-B-M and G-K river sediments.

The Nd–Sr isotopic and clay mineral compositions provide mutually supportive source regime of the detrital components, mixing of G-B-M rivers (~70%) and I-S river sediments (~30%), but minor input of G-K sediments indicated in the K/C ratio. The clay mineral composition reported at the neighboring ODP Site 758 on the NER is notable (Ali et al. 2021). At this site, smectite has been the predominant clay mineral (39~69%) for the last 27 Myrs, which is significantly different from those (23% of smectite and 50% of illite on average) of the study site. Ali et al. (2021) did not, however, apply the weighting factors of Biscaye (1965) for semi-quantitative estimation. It means that the smectite content was overestimated in Ali et al. (2021) like the other data in the EBOB-1 group. Nevertheless, the Nd–Sr isotope compositions of bulk detrital component at ODP 758 site showed excellent agreement with ours (Fig. 4) and support our conclusions on the detrital provenance of the HI1710-MC1 site. Our consistent results suggest that the study site at the NER can serve as an archive for the paleoceanographic studies on the Indian monsoon system, especially, in terms of relative changes in rainfall intensity in the G-B-M rivers and I-S rivers drainage areas, as the site receives its detrital components from these two river systems with different Nd–Sr isotopic and clay mineral compositions.

6 Conclusions

The surface ocean production and detrital provenance of the last 13 kyrs were investigated using a 35 cm-long multiple core retrieved at the northern Ninetyeast Ridge

in the southern Bay of Bengal (BOB). At the study site, surface ocean environment and detrital provenance have not responded sensitively to the Indian Summer Monsoon and largely remained stable for the last 13 kyrs. The small decrease in $CaCO_3$ content was attributed to the strengthened ISM during the mid-Holocene, though not prominent as previously reported in the continental margin sites of the BOB. Radiogenic Sr–Nd isotope and clay mineral compositions indicate two major sources of detrital sediments for the last 13 kyrs: primarily from the Himalaya transported via Ganges–Brahmaputra-Meghna rivers (~ 70%) and secondly from the Indo-Burman Ridges region via Irrawaddy-Salween rivers (~ 30%). This Holocene record provides a basis for the study of Late Quaternary variability in Indian monsoon precipitation pattern, and resultant runoff to the BOB.

Supplementary Information The online version contains supplementary material available at https://doi.org/10.1007/s12601-021-00052-w.

Acknowledgements The authors would like to thank the crew of R/V ISABU and the faculty of LIMS of KIOST for their help. This research was supported by the research program of the KIOST (PE99583, PE9965A), by the National Research Foundation of Korea NRF (2019R1A2C1007701, 2020R1F1A1072239), and by research funds for newly appointed professors of Jeonbuk National University in 2021. The authors would like to thank the editor, Dong-Jin Kang and two anonymous reviewers for their valuable comments.

References

Ahmad SM, Padmakumari VM, Babu GA (2009) Strontium and neodymium isotopic compositions in sediments from Godavari, Krishna and Pennar rivers. Curr Sci India 97:1766–1769

Ali S, Hathorne EC, Frank M, Gebregiorgis D, Stattegger K, Stumpf R, Kutterolf S, Johnson JE, Giosan L (2015) South Asian monsoon history over the past 60 kyr recorded by radiogenic isotopes and clay mineral assemblages in the Andaman Sea. Geochem Geophys Geosyst 16:505–521. https://doi.org/10.1002/2014GC005586

Ali S, Hathorne EC, Frank M (2021) Persistent provenance of South Asian monsoon-induced silicate weathering over the past 27 million years. Paleoceanogr Paleoclimatol 36:e2020PA003909. https://doi.org/10.1029/2020PA003909

Allen R, Najman Y, Carter A, Barfod D, Bickle MJ, Chapman HJ, Garzanti E, Vezzoli G, Andò S, Parrish RR (2008) Provenance of the Tertiary sedimentary rocks of the Indo-Burman Ranges, Burma (Myanmar): Burman arc or Himalayan-derived? J Geol Soc 165:1045–1057. https://doi.org/10.1144/0016-76492007-143

Arrhenius GOS (1952) Sediment cores from tha East Pacific. In: Pettersson H (ed) Reports of the Swedish deep sea expedition, 1947–1948. Swedish Natural Science Research Council, Stockholm, p 201

Banerji US, Arulbalaji P, Padmalal D (2020) Holocene climate variability and Indian Summer Monsoon: an overview. Holocene 30:744–773. https://doi.org/10.1177/0959683619895577

Bejugam P, Nayak GN (2017) Source and depositional processes of the surface sediments and their implications on productivity in recent past off Mahanadi to Pennar River mouths, western Bay of Bengal. Palaeogeogr Palaeoclimatol Palaeoecol 483:58–69. https://doi.org/10.1016/j.palaeo.2016.12.006

Biscaye PE (1965) Mineralogy and sedimentation of recent deep-sea clay in the Atlantic Ocean and Adjacent Seas and Oceans. Geol Soc Am Bull 76:803–832. https://doi.org/10.1130/0016-7606(1965)76[803:masord]2.0.co;2

Bolton CT, Chang L, Clemens S, Kodama K, Ikehara M, Medina-Elizalde M, Paterson GA, Roberts A, Rohling E, Yamamoto Y, Zhao X (2013) A 500,000 year record of Indian summer monsoon dynamics recorded by eastern equatorial Indian Ocean upper water-column structure. Quat Sci Rev 77:167–180. https://doi.org/10.1016/j.quascirev.2013.07.031

Bretschneider L, Hathorne EC, Huang H, Lübbers J, Kochhann KGD, Holbourn A, Kuhnt W, Thiede R, Gebregiorgis D, Giosan L, Frank M (2021) Provenance and weathering of clays delivered to the Bay of Bengal during the middle Miocene: linkages to tectonics and monsoonal climate. Paleoceanogr Paleoclimatol 36:e2020PA003917. https://doi.org/10.1029/2020PA003917

Chapman H, Bickle M, Thaw SH, Thiam HN (2015) Chemical fluxes from time series sampling of the Irrawaddy and Salween Rivers, Myanmar. Chem Geol 401:15–27. https://doi.org/10.1016/j.chemgeo.2015.02.012

Clemens SC, Kuhnt W, LeVay LJ, Anand P, Ando T, Bartol M, Bolton CT, Ding X, Gariboldi K, Giosan L, Hathorne EC, Huang Y, Jaiswal P, Kim S, Kirkpatrick JB, Littler K, Marino G, Martinez P, Naik D, Peketi A, Phillips SC, Robinson MM, Romero OE, Sagar N, Taladay KB, Taylor SN, Thirumalai K, Uramoto G, Usui Y, Wang J, Yamamoto M, Zhou L (2016) Site U1443. In: Clemens SC, Kuhnt W, LeVay LJ, and the Expedition 353 Scientists, Indian Monsoon Rainfall. Proceedings of the International Ocean Discovery Program, 353: College Station, TX (International Ocean Discovery Program). https://doi.org/10.14379/iodp.proc.353.103.2016

Chen Z, Li G (2013) Evolving sources of eolian detritus on the Chinese Loess Plateau since early Miocene: Tectonic and climatic controls. Earth Planet Sci Lett 371–372:220–225. https://doi.org/10.1016/j.epsl.2013.03.044

Chen J, Li G, Yang J, Rao W, Lu H, Balsam W, Sun Y, Ji J (2007) Nd and Sr isotopic characteristics of Chinese deserts: implications for the provenances of Asian dust. Geochim Cosmochim Acta 71:3904–3914. https://doi.org/10.1016/j.gca.2007.04.033

Cheong C-S, Jo HJ, Jeong Y-J, Park C-S, Cho M (2016) Geochemical and Sr–Nd isotopic constraints on the petrogenesis of the Goesan monzodiorite pluton in the central Okcheon belt, Korea. Island Arc 25:43–54. https://doi.org/10.1111/iar.12134

Colin C, Turpin L, Bertaux J, Desprairies A, Kissel C (1999) Erosional history of the Himalayan and Burman ranges during the last two glacial–interglacial cycles. Earth Planet Sci Lett 171:647–660. https://doi.org/10.1016/S0012-821X(99)00184-3

Datta DK, Subramanian V (1997) Texture and mineralogy of sediments from the Ganges-Brahmaputra-Meghna river system in the Bengal Basin, Bangladesh and their environmental implications. Environ Geol 30:181–188. https://doi.org/10.1007/s002540050145

Engleman EE, Jackson LL, Norton DR (1985) Determination of carbonate carbon in geological materials by coulometric titration. Chem Geol 53:125–128. https://doi.org/10.1016/0009-2541(85)90025-7

Farrell JW, Prell WL (1989) Climatic change and $CaCO_3$ preservation: an 800,000 year bathymetric Reconstruction from the central equatorial Pacific Ocean. Paleoceanography 4:447–466. https://doi.org/10.1029/PA004i004p00447

Fleitmann D, Burns SJ, Mudelsee M, Neff U, Kramers J, Mangini A, Matter A (2003) Holocene forcing of the Indian monsoon recorded in a stalagmite from Southern Oman. Science 300:1737. https://doi.org/10.1126/science.1083130

Galy A, France-Lanord C (2001) Higher erosion rates in the Himalaya: geochemical constraints on riverine fluxes. Geology 29:23–26.

https://doi.org/10.1130/0091-7613(2001)029%3c0023:Herith%3e2.0.Co;2
Gebregiorgis D, Hathorne EC, Sijinkumar AV, Nath BN, Nürnberg D, Frank M (2016) South Asian summer monsoon variability during the last ~54 kyrs inferred from surface water salinity and river run off proxies. Quat Sci Rev 138:6–15. https://doi.org/10.1016/j.quascirev.2016.02.012
Giosan L, Naing T, Min Tun M, Clift PD, Filip F, Constantinescu S, Khonde N, Blusztajn J, Buylaert JP, Stevens T, Thwin S (2018) On the Holocene evolution of the Ayeyawady megadelta. Earth Surf Dyn 6:451–466. https://doi.org/10.5194/esurf-6-451-2018
Gourlan AT, Meynadier L, Allègre CJ, Tapponnier P, Birck J-L, Joron J-L (2010) Northern Hemisphere climate control of the Bengali rivers discharge during the past 4 Ma. Quat Sci Rev 29:2484–2498. https://doi.org/10.1016/j.quascirev.2010.05.003
Heaton TJ, Köhler P, Butzin M, Bard E, Reimer RW, Austin WEN, Bronk Ramsey C, Grootes PM, Hughen KA, Kromer B, Reimer PJ, Adkins J, Burke A, Cook MS, Olsen J, Skinner LC (2020) Marine20—the marine radiocarbon age calibration curve (0–55,000 cal BP). Radiocarbon 62:779–820. https://doi.org/10.1017/RDC.2020.68
Hong YT, Hong B, Lin QH, Zhu YX, Shibata Y, Hirota M, Uchida M, Leng XT, Jiang HB, Xu H, Wang H, Yi L (2003) Correlation between Indian Ocean summer monsoon and North Atlantic climate during the Holocene. Earth Planet Sci Lett 211:371–380. https://doi.org/10.1016/S0012-821X(03)00207-3
Hovan SA, Rea DK (1992) The Cenozoic record of continental mineral deposition on broken and ninetyeast ridges, Indian Ocean: Southern African aridity and sediment delivery from the Himalayas. Paleoceanography 7:833–860. https://doi.org/10.1029/92PA02176
Hovan SA (1995) Late Cenozoic atmospheric circulation intensity and climatic history recorded by eolian deposition in the eastern equatorial Pacific Ocean, Leg 138. In: Pisias NG, Mayer LA, Janecek TR, Palmer-Julson A, Vvan Andel TH (eds) Proceedings of the Ocean Drilling Program, Scientific Results. College Station, pp 615–625
Huang X, Zhou T, Dai A, Li H, Li C, Chen X, Lu J, Von Storch J-S, Wu B (2020) South Asian summer monsoon projections constrained by the interdecadal Pacific oscillation. Sci Adv 6:eaay6546. https://doi.org/10.1126/sciadv.aay6546
Hyeong K, Yoo CM, Kim J, Chi S-B, Kim K-H (2006) Flux and grain size variation of eolian dust as a proxy tool for the paleo-position of the Intertropical Convergence Zone in the northeast Pacific. Palaeogeogr Palaeoclimatol Palaeoecol 241:214–223
IPCC (2014) Annex II: Glossary. In: Agard J, Schipper ELF, Birkmann J, Campos M, Dubeux C, Nojiri Y, Olsson L, Osman-Elasha B, Pelling M, Prather MJ, Rivera-Ferre MG, Ruppel OC, Sallenger A, Smith KR, St. Clair AL, Mach KJ, Mastrandrea MD, Bilir TE (eds) Climate Change 2014: Impacts, Adaptation, and Vulnerability. Part B: Regional Aspects. Contribution of Working Group II to the Fifth Assessment Report of the Intergovernmental Panel on Climate Change. Cambridge University Press, Cambridge, pp 1757–1776
Jacobsen SB, Wasserburg GJ (1980) Sm-Nd isotopic evolution of chondrites. Earth Planet Sc Lett 50:139–155. https://doi.org/10.1016/0012-821X(80)90125-9
Jickells TD, An ZS, Andersen KK, Baker AR, Bergametti G, Brooks N, Cao JJ, Boyd PW, Duce RA, Hunter KA, Kawahata H, Kubilay N, laRoche J, Liss PS, Mahowald N, Prospero JM, Ridgwell AJ, Tegen I, Torres R (2005) Global iron connections between desert dust, ocean biogeochemistry, and climate. Science 308:67. https://doi.org/10.1126/science.1105959
Joussain R, Colin C, Liu Z, Meynadier L, Fournier L, Fauquembergue K, Zaragosi S, Schmidt F, Rojas V, Bassinot F (2016) Climatic control of sediment transport from the Himalayas to the proximal NE Bengal Fan during the last glacial-interglacial cycle. Quat Sci Rev 148:1–16. https://doi.org/10.1016/j.quascirev.2016.06.016
Khan MHR, Liu J, Liu S, Seddique AA, Cao L, Rahman A (2019) Clay mineral compositions in surface sediments of the Ganges-Brahmaputra-Meghna river system of Bengal Basin, Bangladesh. Mar Geol 412:27–36. https://doi.org/10.1016/j.margeo.2019.03.007
Kolla V, Bé AWH, Biscaye PE (1976) Calcium carbonate distribution in the surface sediments of the Indian Ocean. J Geophys Res 81:2605–2616. https://doi.org/10.1029/JC081i015p02605
Lee J, Kim S, Lee JI, Cho HG, Phillips SC, Khim B-K (2020) Monsoon-influenced variation of clay mineral compositions and detrital Nd-Sr isotopes in the western Andaman Sea (IODP Site U1447) since the late Miocene. Palaeogeogr Palaeoclimatol Palaeoecol 538:109339. https://doi.org/10.1016/j.palaeo.2019.109339
Li J, Liu S, Shi X, Feng X, Fang X, Cao P, Sun X, Wenxing Y, Khokiattiwong S, Kornkanitnan N (2017) Distributions of clay minerals in surface sediments of the middle Bay of Bengal: source and transport pattern. Cont Shelf Res 145:59–67. https://doi.org/10.1016/j.csr.2017.06.017
Li J, Liu S, Shi X, Zhang H, Fang X, Chen M-T, Cao P, Sun X, Ye W, Wu K, Khokiattiwong S, Kornkanitnan N (2018) Clay minerals and Sr-Nd isotopic composition of the Bay of Bengal sediments: implications for sediment provenance and climate control since 40 ka. Quat Int 493:50–58. https://doi.org/10.1016/j.quaint.2018.06.044
Licht A, France-Lanord C, Reisberg L, Fontaine C, Soe AN, Jaeger J-J (2013) A palaeo Tibet-Myanmar connection? Reconstructing the Late Eocene drainage system of central Myanmar using a multi-proxy approach. J Geol Soc Lond 170:929–939. https://doi.org/10.1144/jgs2012-126
Lupker M, France-Lanord C, Galy V, Lavé J, Kudrass H (2013) Increasing chemical weathering in the Himalayan system since the Last Glacial Maximum. Earth Planet Sci Lett 365:243–252. https://doi.org/10.1016/j.epsl.2013.01.038
Meyers PA (1994) Preservation of elemental and isotopic source identification of sedimentary organic matter. Chem Geol 114:289–302. https://doi.org/10.1016/0009-2541(94)90059-0
Miriyala P, Sukumaran NP, Nath BN, Ramamurty PB, Sijinkumar AV, Vijayagopal B, Ramaswamy V, Sebastian T (2017) Increased chemical weathering during the deglacial to mid-Holocene summer monsoon intensification. Sci Rep 7:44310. https://doi.org/10.1038/srep44310
Mouyen M, Longuevergne L, Steer P, Crave A, Lemoine J-M, Save H, Robin C (2018) Assessing modern river sediment discharge to the ocean using satellite gravimetry. Nat Commun 9:3384. https://doi.org/10.1038/s41467-018-05921-y
Naidu DP, Malmgren BA, Bornmalm L (1993) Quaternary history of calcium carbonate fluctuations in the western equatorial Indian Ocean (Somali Basin). Palaeogeogr Palaeoclimatol Palaeoecol 103:21–30. https://doi.org/10.1016/0031-0182(93)90048-N
Najman Y, Bickle M, BouDagher-Fadel M, Carter A, Garzanti E, Paul M, Wijbrans J, Willett E, Oliver G, Parrish R, Akhter SH, Allen R, Ando S, Chisty E, Reisberg L, Vezzoli G (2008) The Paleogene record of Himalayan erosion: Bengal Basin, Bangladesh. Earth Planet Sci Lett 273:1–14. https://doi.org/10.1016/j.epsl.2008.04.028
Nakai S, Halliday AN, Rea DK (1993) Provenance of dust in the Pacific Ocean. Earth Planet Sci Lett 119:143–157. https://doi.org/10.1016/0012-821X(93)90012-X
Peterson LC, Prell WL (1985) Carbonate preservation and rates of climatic change: an 800 kyr record from the Indian Ocean. In: Sundquist ET, Broecker WS (eds) The carbon cycle and atmospheric CO_2: natural variations Archean to present. American Geophysical Union, Washington, pp 251–269

Phillips SC, Johnson JE, Giosan L, Rose K (2014) Monsoon-influenced variation in productivity and lithogenic sediment flux since 110 ka in the offshore Mahanadi Basin, northern Bay of Bengal. Marine Petrol Geol 58:502–525. https://doi.org/10.1016/j.marpetgeo.2014.05.007

Pickering KT, Carter A, Andò S, Garzanti E, Limonta M, Vezzoli G, Milliken KL (2020) Deciphering relationships between the Nicobar and Bengal submarine fans, Indian Ocean. Earth Planet Sci Lett 544:116329. https://doi.org/10.1016/j.epsl.2020.116329

Rixen T, Gaye B, Emeis KC, Ramaswamy V (2019) The ballast effect of lithogenic matter and its influences on the carbon fluxes in the Indian Ocean. Biogeosciences 16:485–503. https://doi.org/10.5194/bg-16-485-2019

Rodolfo KS (1969) Sediments of the Andaman Basin, northeastern Indian Ocean. Mar Geol 7:371–402. https://doi.org/10.1016/0025-3227(69)90014-0

Sager WW, Paul CF, Krishna KS, Pringle M, Eisin AE, Frey FA, Gopala Rao D, Levchenko O (2010) Large fault fabric of the Ninetyeast Ridge implies near-spreading ridge formation. Geophys Res Lett 37:L17304. https://doi.org/10.1029/2010GL044347

Schlitzer R (2021) Ocean data view. https://odv.awi.de/ Accessed 25 Aug 2021

Si N, Halliday AN, Rea DK (1993) Provenance of dust in the Pacific Ocean. Earth Planet Sci Lett 119:143–157

Sijinkumar AV, Clemens S, Nath BN, Prell W, Benshila R, Lengaigne M (2016) $\delta^{18}O$ and salinity variability from the Last Glacial Maximum to Recent in the Bay of Bengal and Andaman Sea. Quat Sci Rev 135:79–91. https://doi.org/10.1016/j.quascirev.2016.01.022

Singh SK, France-Lanord C (2002) Tracing the distribution of erosion in the Brahmaputra watershed from isotopic compositions of stream sediments. Earth Planet Sci Lett 202:645–662. https://doi.org/10.1016/S0012-821X(02)00822-1

Singh SK, Rai SK, Krishnaswami S (2008) Sr and Nd isotopes in river sediments from the Ganga Basin: sediment provenance and spatial variability in physical erosion. J Geophys Res Earth Surf. https://doi.org/10.1029/2007JF000909

Song Z, Wan S, Colin C, Yu Z, Révillon S, Jin H, Zhang J, Zhao D, Shi X, Li A (2021) Paleoenvironmental evolution of South Asia and its link to Himalayan uplift and climatic change since the late Eocene. Glob Planet Change 200:103459. https://doi.org/10.1016/j.gloplacha.2021.103459

Southon J, Kashgarian M, Fontugne M, Metivier B, Yim W-S (2002) Marine reservoir corrections for the Indian Ocean and Southeast Asia. Radiocarbon 44:167–180. https://doi.org/10.1017/S0033822200064778

Stuiver M, Reimer PJ, Reimer RW (2021) CALIB 8.2 [WWW program]. http://calib.org. Accessed 3 Aug 2021

Stuiver M, Reimer PJ (1993) Extended 14C data base and revised CALIB 3.0 ^{14}C Age Calibration Program. Radiocarbon 35:215–230. https://doi.org/10.1017/S0033822200013904

Sun X, Liu S, Fang X, Li J, Cao P, Zhao G, Khokiattiwong S, Kornkanitnan N, Shi X (2020) Clay minerals of surface sediments from the lower Bengal Fan: implications for provenance identification and transport processes. Geol J 55:6038–6048. https://doi.org/10.1002/gj.3786

Suresh N, Bagati TN (1998) Calcium carbonate distribution in the Late Quaternary sediments of Bay of Bengal. Curr Sci India 74:977–984

Tripathy GR, Singh SK, Bhushan R, Ramaswamy V (2011) Sr–Nd isotope composition of the Bay of Bengal sediments: Impact of climate on erosion in the Himalaya. Geochem J 45:175–186. https://doi.org/10.2343/geochemj.1.0112

Turner AG, Annamalai H (2012) Climate change and the South Asian summer monsoon. Nat Clim Change 2:587–595. https://doi.org/10.1038/nclimate1495

Zweng MM, Reagan JR, Seidov D, Boyer TP, Locarnini RA, Garcia HE, Mishonov AV, Baranova OK, Weathers KA, Paver CR, Smolyar I (2018) World ocean Atlas 2018, volume 2: salinity. NOAA Atlas NESDIS 82:50